THE JOURNAL OF PHYSICAL CHEMISTRY C
ARTICLE
pubs.acs.org/JPCC

Directional Enhancement of Spontaneous Emission in Polymer Flexible Microcavities

L. Frezza,[†,§] M. Patrini,[‡] M. Liscidini,[‡] and D. Comoretto*[,†]

[†]Dipartimento di Chimica e Chimica Industriale, Università degli Studi di Genova, Via Dodecaneso 31, I-16146 Genova, Italy
[‡]Dipartimento di Fisica "A. Volta", Università degli Studi di Pavia, Via Bassi 6, I27100 Pavia, Italy

ABSTRACT: We report on the control of spontaneous emission in flexible polymer 1D photonic crystal cavities fabricated by spin coating having a layer of poly(9,9-dioctylfluorenyl-2,7-diyl-*co*-1,4-benzo-(2,1′-3)-thiadiazole) (F8BT) as an active material. The optical properties of these full-polymer photonic crystals are systematically investigated by means of polarized angular-resolved transmittance and photoluminescence spectral measurements. We demonstrate strong directional emission enhancement when the emitter is located in the defect layer and resonantly coupled to the microcavity mode. The experimental results can be successfully reproduced with different theoretical optical models.

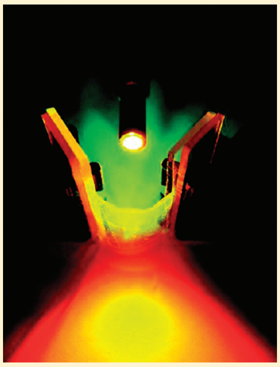

1. INTRODUCTION

Photonic crystal (PhC) structures are characterized by a periodic modulation of the dielectric function on a scale comparable to the wavelength of interest. Such a modulation allows for the control of the photon dispersion relation and the creation of photonic band gaps (PBGs), that is, frequency ranges for which light propagation in one or more directions is forbidden.[1] Through a careful design of a PhC, it is also possible to achieve light confinement and extremely high electromagnetic field enhancement by inserting "ad hoc" structural/dielectric defects in the periodic structure.

Since the pioneering work by Yablonovitch,[2] the control of light emission has been indicated as one of the most interesting and promising applications of PhC structures.[2,3] In particular, suppression, enhancement, or redistribution of spontaneous emission have been and are subjects of intensive investigations.[4−8] In this regard, 1D photonic microcavities have been studied in the framework of spontaneous emission control and, more in general, light−matter interaction.[9] A 1D PhC microcavity is constituted of a defect layer sandwiched between two multilayers (distributed Bragg reflectors, DBRs) that are dielectric mirrors, that is, 1D PhC (Figure 1a). Semiconductor and oxide periodic multilayers have been studied for over 30 years in the fields of linear and nonlinear optics.[10−12] Although these structures are simple regular stacks of layers of different materials, their growth/fabrication can be time- and cost-expensive depending on the material choice and the operation wavelength, which defines the typical layer thicknesses.

In this scenario, polymers have been able to attract a growing interest because of their peculiar optical, mechanical, and processing properties. As a matter of fact, polymer PhC can be prepared by exploiting spontaneous self-assembly of suitable block copolymers or by spin-coating. At present, block copolymers PhC find major application as color-responsive sensors in wet environment,[13−21] whereas strictly photonic studies are performed with spin-cast structures. Indeed, enhancement of second-harmonic generation of thin polymer films embedded in a dielectric microcavity,[22] light-emitting diodes using all-polymer microcavities,[23] and distributed-feedback dye lasing in a polymer multilayer[24−26] have been demonstrated. Different fabrication methods of polymer DBR and planar microcavities have been investigated by several authors to achieve a suitable dielectric contrast, to retain an easy processability and chemical compatibility of macromolecular components, and to allow their chemical doping with the desired photoactive material. Fluorocarbon polymers have been used to obtain a relatively large dielectric contrast. However, the limited processability of such polymers requires a sophisticated deposition technique (ion-beam sputtering), which is not compatible with low-cost devices and with processing of conjugated semiconductors or of other organic/hybrid active media.[27−29] The use of coextrusion methods, widely adopted in industrial plants, has been demonstrated to produce polymer multilayers[30] but has not been extensively applied for photonic applications.

The spin-coating techniques are instead very powerful to obtain polymer DBR structures because they require only the use of macromolecules or colloids possessing a significant dielectric contrast, which could be dissolved in orthogonal solvents.[8,31−34] The possibility of fabricating high optical quality

Received: June 28, 2011
Revised: August 31, 2011
Published: August 31, 2011

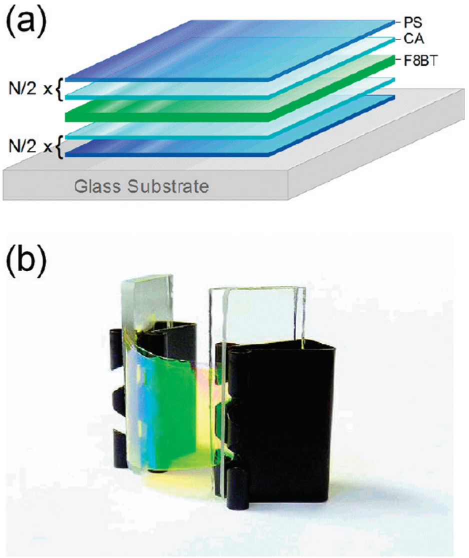

Figure 1. (a) 1D PhC microcavity structure layout. (b) Image of a flexible microcavity.

polymer multilayers by spin coating significantly decreases the fabrication cost in a number of applications and introduces mechanical flexibility as an added value, avoiding the need for a stiff substrate. (See Figure 1b.) Moreover, such structures are not limited to work in a wet environment like those made of block copolymers. Finally, spin-cast PhC structures have the advantage of being easily doped with both photoactive organic or colloidal semiconductors. Indeed, they have been used to achieve amplified spontaneous emission or lasing action at the PBG edge where an increase in the density of photonic states (DOS) is obtained as a result of the flat band condition[24,26,35−37] because the DOS is inversely proportional to the photon group velocity, which is directly proportional to the first derivative of the photon dispersion (i.e., the band structure) along the propagation direction. This condition also allows us to achieve directional enhancement effects of the photoluminescence (PL) spectrum, as demonstrated for dye-doped colloidal photonic crystals,[4−7,38] and light localization effects on the absorption properties of opals doped with gold nanoparticles.[39,40]

In the field of photonics, a more exciting way to tune the photonic DOS is provided by the introduction of structural defects where the active material is embedded.[41] Such engineered systems allow an efficient light confinement with respect to the bare periodic structure of a PhC and can be tailored to specific shapes and dielectric properties. A typical example of a structural photonic defect in a 1D system is a planar microcavity where two DBR mirrors are separated by a defect layer, which breaks the DBR periodicity.[42,43] Several types of similar structures made out of inorganic semiconductors have been investigated in the past.[44,45] More recently, *organic* semiconductors have been exploited as defect layers within an *inorganic* DBR,[12,46−54] whereas only a few papers instead deal with *all-polymer* microcavities.[25]

In this work, we present a systematic study of flexible polystyrene/cellulose acetate (PS/CA) 1D photonic crystal microcavities engineered with F8BT as the light-emitting defect layer. We demonstrate that high-quality photonic crystal structures can be fabricated by spin-coating, and we show a very precise control over the multilayer structure and thicknesses. In particular, we study their optical response by means of reflectance, angle-resolved transmittance, and PL measurements, comparing experimental data with both numerical calculations and best-fit simulations. Directional enhancement of spontaneous emission by the F8BT defect layer is demonstrated in the visible spectral interval, where both the spectral position of the PBG and the cavity mode can be finely tuned.

2. EXPERIMENTAL METHODS

Polystyrene (M_w = 200 000) and cellulose acetate (M_w = 61 000) used for multilayer growth were purchased from Sigma-Aldrich and used without further purification. Poly(9,9-dioctylfluorenyl-2,7-diyl-*co*-1,4-benzo-(2,1′-3)-thiadiazole) was purchased from American Dye Source (ADS133YE), and its molecular mass is unknown. Toluene and diacetonalcohol (4-hydroxy-4-methyl-2-penthanon) were used to prepare polymer solutions with a concentration of few milligrams per milliliter.

The growth of polystyrene and cellulose acetate multilayers was performed by dynamic spin-coating (Novocontrol spinner model SCV) over glass substrates in laboratory environment without temperature or humidity control. No baking of cast films was performed. Layer thickness was selected by changing the spinning speed (∼100 revolutions per second) and solution concentrations. The samples analyzed in this work were $(PS/CA)_N$ multilayers with N = 15, 25, 30. The nominal layer thicknesses were 85 and 90 nm for PS and CA layers, respectively. These values were chosen to realize a $\lambda/4$ DBR at ∼550 nm, where F8BT polymer shows maximum fluorescence emission.

The F8BT microcavity was obtained by spinning the relative toluene solution over a multilayer made of 15 pairs of PS-CA films. Then, an additional 15 CA-PS bilayers were grown over the F8BT film to complete the structure, which is sketched in Figure 1a. An image of a free-standing flexible sample with 30-period DBR peeled off the glass substrate is shown in Figure 1b. Note that the repeatability of layer deposition is a crucial issue to obtain good DBR because optical transmittance and reflectance response critically depend on the layer thickness and periodicity. Sample uniformity and thickness check over large areas (2.5 × 2.5 cm^2) has been performed by an Avantes compact spectrometer equipped with an optical fiber reflection stage and by using the AvaSoft-Thinfilm software. This software allowed for a first rough evaluation of DBR films thickness useful to determine the lambda/4 condition, which can then be finely tuned by slightly modifying the spinning speed. A posteriori determination of real thicknesses for top quality samples was obtained by ellipsometry and modeling: the discrepancy between nominal and real values was found to be within 5% (see below).

Angle-resolved transmittance spectra for both s- and p-polarizations were measured with a setup previously described[6] and also used for PL measurements at variable collection angle.

In addition, reflectance and transmittance at near-normal incidence were measured in the 0.2 to 1.6 μm range (UV−vis−NIR) using a Varian Cary 6000i spectrophotometer with a photometric accuracy of 0.5% and spectral resolution better than 0.2% of the wavelength. Using a V−W accessory and an Al mirror as a reference, we also obtained the absolute values of R at normal incidence.

Spectroscopic ellipsometry was used to obtain the optical functions and thicknesses of polymer layers used to prepare the microcavities. Ellipsometric spectra in the 0.25 to 0.9 μm range

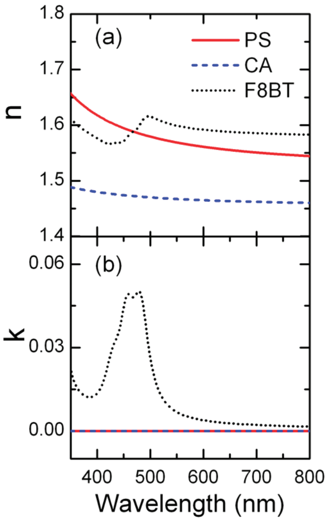

Figure 2. Polymer optical functions: (a) refractive index, *n*, and (b) extinction coefficient, *k*.

were measured by an automatic ellipsometer Sopra MOSS ES4G. The system uses a rotating polarizer, an autotracking analyzer, a double monochromator, and a single-photon-counting photomultiplier detector system. SE spectra were acquired with a spectral resolution of 1 nm and at different angles of incidence from 60 to 75°, close to the Brewster angle of the different materials for optimum sensitivity. Glass and silicon substrates were previously characterized by determining their optical functions and native oxide thickness.

R, T, and SE experimental spectra were modeled with WVASE32 software by J. A. Woollam, which uses the Levenberg—Marquardt algorithm for fitting. To test compositional and thickness uniformity of spin-cast layers, we performed measurements on different points of the surface. The spectra from different points coincide within experimental uncertainty so that the samples can be considered to be laterally homogeneous.

The design and modeling of the multilayers were performed by means of the transfer matrix method,[10] which allows calculating reflectance and transmission spectra as a function of the angle of incidence and input light polarization. In the calculations, we take into account the refractive index dispersion of the constituent materials by using the dielectric functions obtained from ellipsometric data.

3. RESULTS AND DISCUSSION

Sample preparation and characterization techniques are reported in the Experimental Methods section. Here we show the optical and spectroscopic properties of DBR and microcavities through angle-resolved transmittance (T), reflectance (R), and spectroscopic ellipsometry (SE), and we compare the experimental results to the numerical calculations and simulations. Then, we present experimental results on the control of spontaneous PL emission from the F8BT defect layer.

3.1. Complex Refractive Index of Polymer Materials. The complex refractive index ($n + ik$; n, refractive index; k, extinction coefficient) of DBR composing materials is one of the main parameters governing the optical response of a PhC. Being polymers usually transparent, only n values are usually reported in polymer atlas and often neglecting its wavelength dispersion.[55]

Table 1. Best-Fit Sellmeier Parameters (See Equation 1) for PS, CA, and F8BT (* for $\lambda > 500$ nm) Refractive Index Dispersion

	A	*B*	*C* (μm)
PS	1.3393	0.9863	0.1913
CA	0.6138	1.4994	0.0896
F8BT*	2.4415	0.0454	0.4288

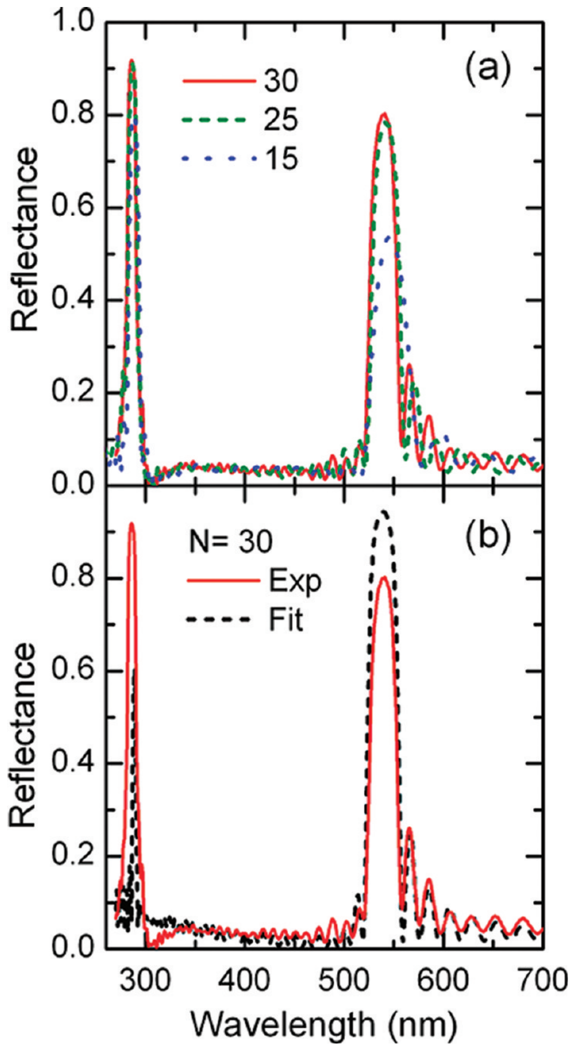

Figure 3. (a) DBR reflectance spectra at normal incidence as a function of the number N of periods. (b) Reflectance spectrum of the $N = 30$ sample and corresponding best-fit simulation.

Even though some results on the optical characterization of PS and CA have been reported,[56] their optical functions are known to depend on the polymer mass, solvent, and deposition conditions (density). For these reasons, we first performed an ellipsometric study of the complex refractive index of several PS and CA spin-cast films (on silicon wafers and glass substrates) with thickness ranging from 80 to 250 nm and from 50 to 1090 nm, respectively. This activity allowed us to (i) check the optical quality and uniformity of the spin-cast polymer layers, (ii) compare the optical response of the multilayer structures with that derived on the basis of simulation models, in particular, their

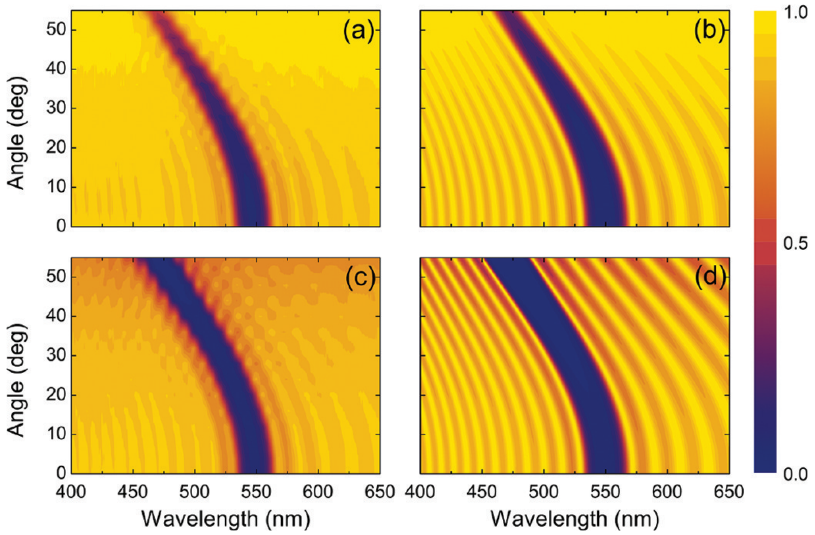

Figure 4. Thirty-period DBR transmittance spectra as a function of the angle of incidence for s-polarized ((a) experiment and (b) theory) and p-polarized ((c) experiment and (d) theory) incident light.

behavior as 1D photonic crystals, and (iii) verify the correspondence between actual and nominal structure parameters.

In Figure 2a, we report the refractive index spectra for PS and CA, as obtained by the simultaneous best-fit procedure on reflectance, transmittance, and spectroscopic ellipsometry spectra of polymer single layers. Free parameters of the best-fit were the refractive index dispersion and the film thickness values. The refractive index dispersion has been modeled by the Sellmeier relation[57]

$$n^2 = A + B\frac{\lambda^2}{\lambda^2 - C^2} \qquad (1)$$

where A, B, and C are fit parameters. Their values for PS and CA are summarized in Table 1.

The PS refractive index dispersion is comparable to that reported in literature for materials of similar molecular weight after sample baking at 100 °C for 10 min.[56] For what concerns CA, we cannot make a direct comparison to literature data because they depend on the degree of hydroxylation and processing conditions. Values for the refractive index in the range 1.46 to 1.50 have been reported[58] for cellulose triacetate in full agreement with our findings.

The same procedure has been applied, in the transparency spectral interval (500−900 nm), to F8BT films having thickness similar to that used for microcavities, thus allowing us to derive the refractive index dispersion and the actual thickness values. Best-fit Sellemeier parameters for F8BT are also reported in Table 1. At lower wavelengths, where the electronic absorption of F8BT rises, a numerical inversion of the SE spectra has been performed, deriving dispersion properties of both n and k (Figures 2a and b). These optical functions well reproduce normal incidence T spectra of the same layers on glass substrates. We note the characteristic F8BT absorption feature at ∼490 nm (and the corresponding dispersion feature in the n spectrum), which is responsible for the absorption band observed in the transmittance spectra of the microcavity (shown below).

We notice that the optical functions so far derived for F8BT do not show evidence of uniaxial anisotropy, as previously found by Ramsdale et al. in annealed films of the same polymer of comparable thickness, which showed preferential alignment of the macromolecules in the plane of the film.[59] This discrepancy can be ascribed to the well-known dependence of the optical response of F8BT on the molecular mass and processing conditions.[60]

3.2. Optical Response and Modeling of Polymer DBR Structures. The PS and CA optical functions so far determined have been used to design DBR structures and microcavities as well as to calculate the R spectra by both the simulation and the best-fit procedures for DBR having a different number of periods (N = 15, 25, 30; Figure 3a). Two major features are evident at about λ = 540 and 280 nm due to constructive interference of light diffracted by each interface inside the multilayer. These reflectance bands (i.e., minima in the T spectra, see below) are associated with the first- and second-order gaps of the corresponding 1D photonic structure. Several side oscillations are also evident in the R spectra due to the typical Fabry−Perot interference of the multilayer. By increasing the number of periods, the stop-bands become sharper, and their intensity increases toward unity, whereas the oscillations are decreasing in intensity due to a more effective destructive interference (Figure 3a).

A typical best-fit curve to the R spectrum is shown in Figure 3b for the sample with N = 30 periods. PS and CA layer thicknesses from the best-fit are 86.5 and 91 nm, respectively, producing a first-order stop band peaked at λ = 540 nm with full width at half-maximum of $\Delta\lambda$ = 28 nm. These results compare well with the designed structure with a variation from the nominal layer thickness of <5%. Notice that this accuracy in the thickness control, remarkable for a simple technique like spinning, allows us a fine-tuning the PBG of the structures at any desired wavelength. Indeed, we successfully obtained DBR with PBG ranging from 300 to 1800 nm.

It is worthy noticing that the multilayers are designed to be quarter-wavelength stacks at λ = 550 nm. This condition gives the largest achievable first order stop-band, whereas no second-order stop-band is expected when the material dispersion is neglected. The appearance of the second-order stop band at 280 nm indicates the importance of taking into account the wavelength dependence of the material refractive index. The agreement between experimental data and simulations confirms

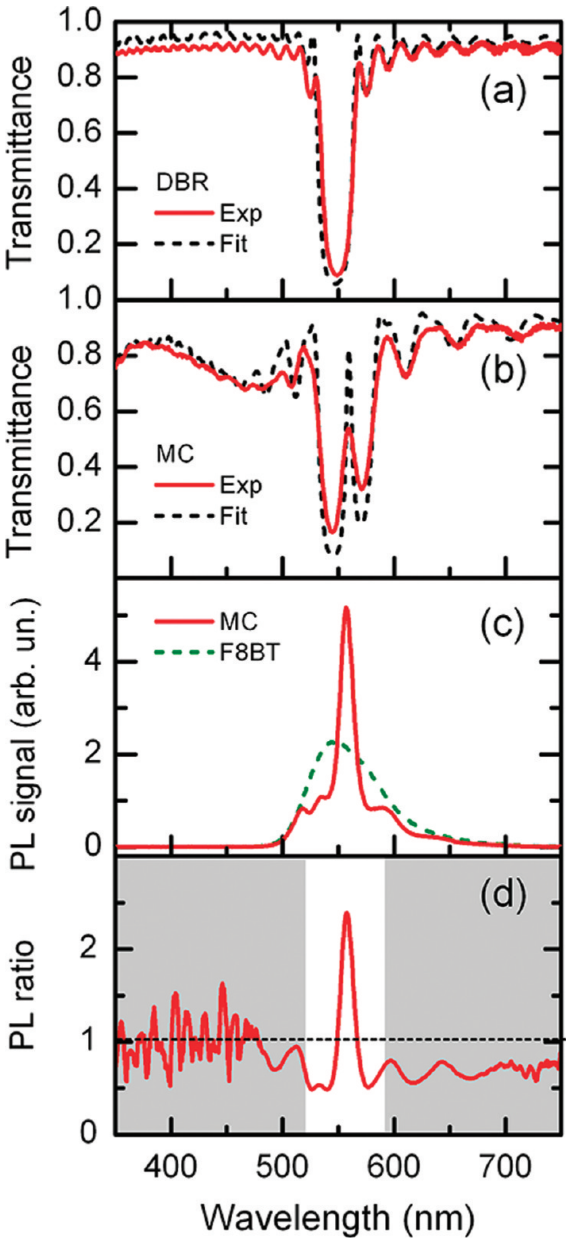

Figure 5. (a) Transmittance of the DBR sample with $N = 30$ periods (solid) and best-fit spectrum (dashed). (b) Microcavity (MC) transmittance (solid) and corresponding best-fit spectrum (dashed). (c) Photoluminescence spectrum of the MC at normal collection (solid) and of the bare F8BT defect layer (dashed). (d) Ratio of the PL spectra reported in panel c. The undashed region corresponds to the photonic band gap.

not only the good optical quality of these structures, but also the accuracy of the ellipsometric data in describing the materials' refractive index dispersion.

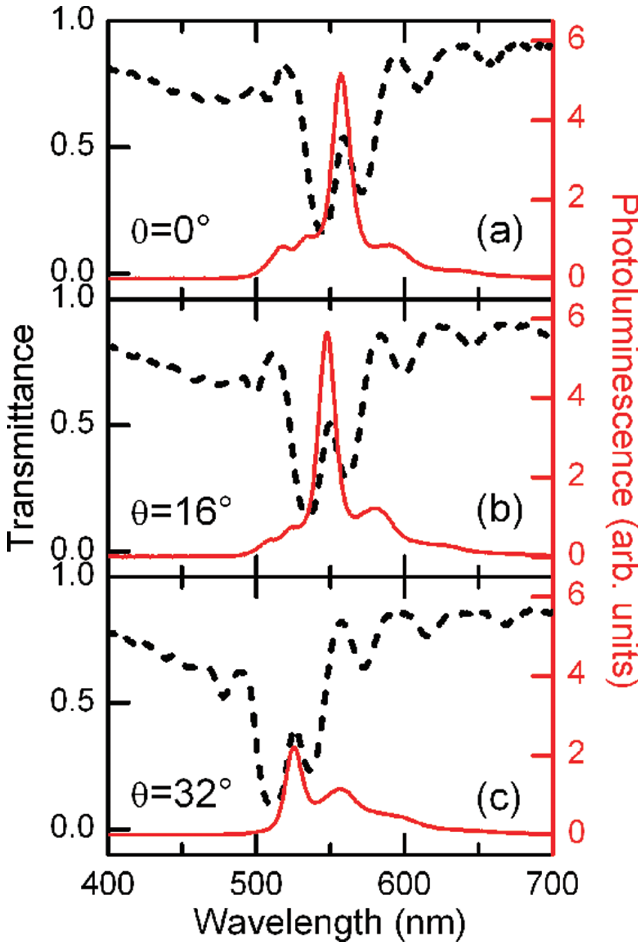

Figure 6. Experimental MC transmittance (dashed) and photoluminescence (solid) spectra at three different angles of incidence/collection: (a) 0, (b) 16, and (c) 32°.

We also investigated the angular dispersion of the main stop band to highlight its polarization dependence. To this end, we performed polarized T measurements, and we compared them with the calculated spectra. In Figure 4, we report contour plots of T intensity of a DBR ($N = 30$) for s-polarized and p-polarized light, which show a slight polarization-dependent dispersion and a remarkable difference for the PBG width. A very good agreement between experiment and theoretical calculations is observed, thus confirming the high optical quality of our PhC structures grown by spin-coating with a pair of polymers having a relatively low dielectric contrast. Notice also that the side oscillations to stop-band optical intensity, which are indicative of the finite size effects of the periodic structure, could be further optimized by increasing the number of periods or improving the homogeneity of the different layers. We notice that the observed dispersion allows us to exploit the angle of incidence and the light polarization as additional tuning parameters to operate at the preferred experimental configuration. From the application point of view, these tunings could also be achieved by exploiting the mechanical flexibility of the free-standing structures (as observed in Figure 1b), which can be properly bent and shaped when peeled off from the substrate.

3.3. Introducing an Optically Active Structural Defect in the DBR: Tuning of Spontaneous Emission Spectra. After the characterization of the polymer DBR structure, we embedded a structural and dielectric F8BT defect layer between two identical multilayers. The PhC is designed so that the PL spectrum of F8BT, centered at $\lambda = 550$ nm, is spectrally overlapped to the multilayer stop band. The effect of the F8BT defect on the normal incidence T spectra of the overall structure is reported in Figure 5b and there compared with those of the bare multilayer (Figure 5a). We observe the appearance of a peak in the center of the band gap and of the F8BT absorption band around $\lambda = 460$ nm, which modifies the overall interference pattern. The peak is the optical fingerprint of the presence of a defect in the PhC structure. We also succeeded in tuning the spectral position of the defect mode within the band gap by changing the thickness of the defect layer as theoretically predicted.[61] The spectral position and intensity of the defect mode are well-reproduced by the simulation model, by adopting the dielectric functions, the multilayer period, and the defect layer thickness previously determined.

The line width of the defect mode (at λ = 559 nm) is a parameter that defines the quality factor of an optical cavity mode $Q = \lambda/\Delta\lambda$. In the present case, Q is ~50, which favorably compares with data (~70) reported in the literature for polymer microcavities having a larger dielectric contrast.[25] Note that in the present work the cavity quality factor has not been optimized. Larger values (for the present dielectric contrast) could, in principle, be obtained by increasing the number of periods of the DBR.

In Figure 5c, the PL spectra at normal collection angle of a bare F8BT film and of a MC are reported. We notice that in the two samples the thickness of the F8BT layer is identical. The F8BT PL spectrum shows a broad band centered at λ = 544 nm, in agreement with previous findings.[62] As soon as the active layer is embedded in the multilayer structure, its PL spectrum is strongly modified, showing a sharp peak at λ = 557 nm with reduced line width of ~13 nm, with side features within the bandgap. We underline that the sharp PL peak spectrally matches the defect mode observed in the T spectrum of the MC, whereas the side wings precisely overlap to the whole band gap structure (Figure 5b). Outside the band gap spectral region, the PL spectra of both F8BT film and microcavity coincide and show almost the same intensity. This last observation allows us to establish an intensity reference to discuss quantitatively the role of PhC band gap on the PL spontaneous emission, as recently demonstrated on opals doped with fluorescent chromophores.[4,6,38]

The spectral and intensity modification of F8BT PL are better highlighted in Figure 5d, where the ratio of the PL MC spectrum to that of bare F8BT film is reported. We focus our attention to the spectral region of the PBG (undashed area). On the one hand, the F8BT PL spectrum is suppressed within the band gap with respect to the reference because the propagation of such photons is forbidden. On the other hand, a significant increase in PL intensity is observed in correspondence of the defect mode. Indeed, the PhC structure confines the electromagnetic field inside the cavity, promoting the strong interaction of the electromagnetic field with the active layer as a consequence of the spectral and spatial coupling of the emitter with the cavity mode. By evaluating the integral of the PL spectra of Figure 5c, we obtain almost the same value, thus indicating that the role of the PhC is mainly a spatial redistribution of the emitted light.

This spectral coincidence between PL and PhC band gap features is further confirmed by analyzing the dependence of PL spectra measured at different collection angles (Figure 6), there compared with the corresponding T response.

The PBG and cavity mode dispersions observed in the T spectra are analogous to that of the bare multilayer discussed in Figure 4. The defect PL peak strictly follows the band gap dispersion, thus demonstrating the one-to-one correspondence between PL intensity redistribution and PhC features. In particular, in Figure 7, we plot the angular and spectral map of the MC emission, clearly evidencing the directional enhancement of the PL signal. From the above results it is evident that a PhC band gap dispersion matched to a specific emissive material allows us to obtain PL enhancement for a wide spectral and angular range, thus finding applications in the control and enhancement of the emission, for example, in low-threshold flexible lasing devices.[25]

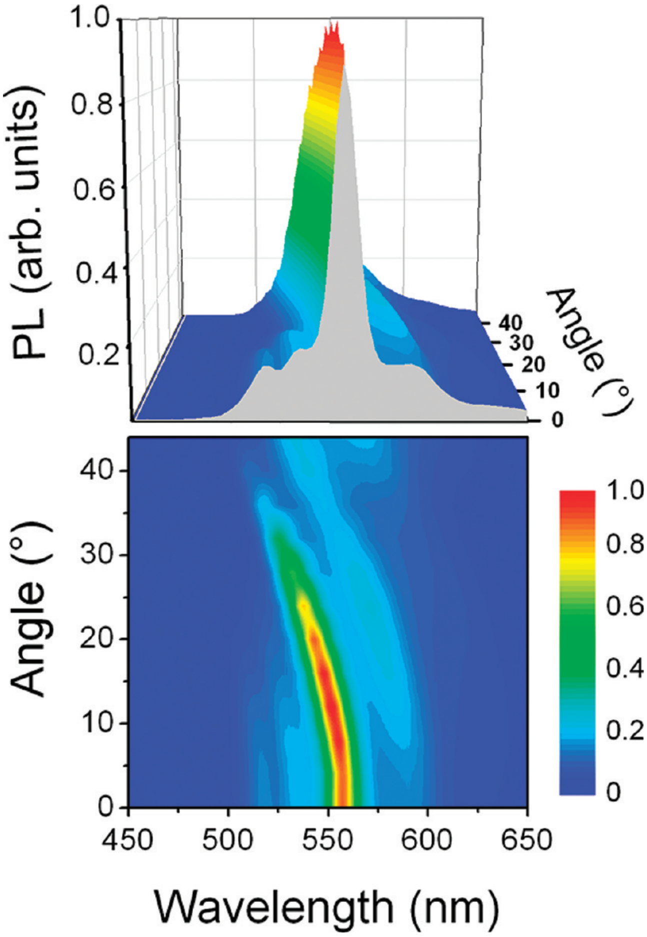

Figure 7. MC photoluminescence spectra as a function of the collection angle (a) and PL signal intensity contour plot (b).

4. CONCLUSIONS

We demonstrated that the spin-coating technique is a very powerful tool for preparing all-polymer, flexible microcavities of high optical quality having a control over critical thicknesses below 5%. We determined the optical functions of constituent materials, thus allowing a precise design of the microcavity structure and the accurate modeling of its optical response. We prepared high-quality DBR operating in the visible range and microcavities containing a photoactive F8BT layer as the structural defect. Then, the comparison of the F8BT PL spectra of microcavities with those of bare polymer shows a remarkable enhancement of the emission intensity for cavity modes, whereas a PL reduction is observed within the PBG. The PL angular dispersion properties fully agree with those of transmittance spectra, thus demonstrating a directional and spectral redistribution of PL emission due to the tuning of the photonic band structure by structural defects. In addition to the microcavity structure design, finer tuning of the PL wavelength can be achieved by angular selection in the signal collection geometry, sample bending, or both.

The unprecedented control of active and passive optical properties of polymer multilayers and microcavities makes these systems a valuable, simple, and cheap platform where material science and photonics merge to respond to a variety of technological needs. We envisage their use in a number of applications ranging from photonics to sensing and photovoltaics.

AUTHOR INFORMATION

Corresponding Author

*Tel: +39-0103538736. Fax: +39-0103538733. E-mail: davide.comoretto@unige.it.

Present Addresses

[§]Center for Nano Science and Technology (CNST) of IIT@PoliMi, Istituto Italiano di Tecnologia (IIT), Via Pascoli 70/3, 20133 Milano, Italy.

ACKNOWLEDGMENT

Work in Genova is partially supported by Fondazione Cariplo through the project "PHOtonic ENhancement In Chemical Sensors: nanomaterials for optics (PHOENICS)". Work in Pavia is partially supported by Regione Lombardia through the project "Nanostructured photonic devices for innovative biosensing applications" (ID 16785).

REFERENCES

(1) John, S. *Phys. Rev. Lett.* **1987**, *58*, 2486–2489.

(2) Yablonovitch, E. *Phys. Rev. Lett.* **1987**, *58*, 2059–2062.

(3) Joannopulos, J. D.; Meade, R. D.; Win, J. N. *Photonic Crystals: Molding the Flow of the Light*; Princeton University Press: Princeton, NJ, 1995.

(4) Barth, M.; Gruber, A.; Cichos, F. *Phys. Rev. B* **2005**, *72*, 085129.

(5) Lodhal, P.; vanDriel, A. F.; Nikolaev, I. S.; Irman, A.; Overgaag, K.; Vanmaekelbergh, D.; Vos, W. L. *Nature* **2004**, *430*, 654–657.

(6) Berti, L.; Cucini, M.; Di Stasio, F.; Comoretto, D.; Galli, M.; Marabelli, F.; Manfredi, N.; Marinzi, C.; Abbotto, A. *J. Phys. Chem. C* **2010**, *114*, 2403–2413.

(7) Kubo, S.; Fujishima, A.; Sato, O.; Segawa, H. *J. Phys. Chem. C* **2009**, *113*, 11704–11711.

(8) Sanchez-Sobrado, O.; Calvo, M. E.; Nunez, N.; Ocana, M.; Lozano, G.; Miguez, H. *Nanoscale* **2010**, *2*, 936–941.

(9) Björk, G.; Machida, S.; Yamamoto, Y.; Igeta, K. *Phys. Rev. A* **1991**, *44*, 669–681.

(10) Yariv, A.; Yeh, P. *Optical Waves in Crystals*; Wiley: Hoboken, NJ, 2003.

(11) Lozano, G.; Colodrero, S.; Caulier, O.; Calvo, M. E.; Miguez, H. *J. Phys. Chem. C* **2010**, *114*, 3681–3687.

(12) Tessler, N.; Denton, G. J.; Friend, R. H. *Nature* **1996**, *382*, 695–697.

(13) Cavallo, D.; Comoretto, D. In *Ionic Interactions in Natural and Synthetic Macromolecules*; Ciferri, A., Perico, A., Eds.; John Wiley & Sons: Hoboken, NJ, 2011, in press.

(14) Kang, Y.; Walish, J. J.; Gorishnyy, T.; Thomas, E. L. *Nat. Mater.* **2007**, *6*, 957–960.

(15) Kang, C.; Kim, E.; Baek, H.; Hwang, K.; Kwak, D.; Kang, Y.; Thomas, E. L. *J. Am. Chem. Soc.* **2009**, *131*, 7538–7539.

(16) Park, C.; Yoon, J.; Thomas, E. L. *Polymer* **2003**, *44*, 6725–6760.

(17) Valkama, S.; Kosonen, H.; Ruokolainen, J.; Haatainen, T.; Torkkeli, M.; Serimaa, R.; Brinke, G.t.; Ikkala, O. *Nat. Mater.* **2004**, *3*, 872–876.

(18) Hustad, P. D.; Marchand, G. R.; Garcia-Meitin, E. I.; Roberts, P. L.; Weinhold, J. D. *Macromolecules* **2009**, *42*, 3788–3794.

(19) Parnell, A. J.; Tzokova, N.; Pryke, A.; Howse, J. R.; Mykhaylyk, O. O.; Ryan, A. J.; Panine, P.; Fairclough, J. P. A. *Phy. Chem. Chem. Phys.* **2011**, *13*, 3179–3186.

(20) Parnell, A. J.; Pryke, A.; Mykhaylyk, O. O.; Howse, J. R.; Adawi, A. M. A.; Terril, N. J.; Fairclough, J. P. A. *Soft Matter* **2011**, *7*, 3721–3725.

(21) Guldin, S.; Kolle, M.; Stefik, M.; Langford, R.; Eder, D.; Wiesner, U.; Steiner, U. *Adv. Mater.* **2011**, *23*, 3664–3668.

(22) Cao, H.; Hall, D. B.; Torkeison, J. M.; Cao, C. Q. *Appl. Phys. Lett.* **2000**, *76*, 538–540.

(23) Hou, L.; H., Q.; Mo, Y.; Peng, J.; Cao, Y. *Appl. Phys. Lett.* **2005**, *87*, 243504.

(24) Komikado, T.; Yoshida, S.; Umegaki, S. *Appl. Phys. Lett.* **2006**, *89*, 061123.

(25) Menon, V. M.; Luberto, M.; Valappil, N. V.; Chatterjee, S. *Opt. Express* **2008**, *16*, 19535–19540.

(26) Scotognella, F.; Monguzzi, A.; Meinardi, F.; Tubino, R. *Phys. Chem. Chem. Phys.* **2010**, *12*, 337–340.

(27) Quaranta, F.; Valentini, A.; Favia, P.; Lamendola, R.; d'Agostino, R. *Appl. Phys. Lett.* **1993**, *63*, 10–11.

(28) Convertino, A.; Valentini, A.; Ligonzo, T.; Cingolani, R. *Appl. Phys. Lett.* **1997**, *71*, 732–734.

(29) Convertino, A.; Valentini, A.; Cingolani, R. *Appl. Phys. Lett.* **1999**, *75*, 322–324.

(30) Sandrock, M.; Wiggins, M.; Shirrk, J. S.; Tai, H.; Ranade, A.; Baer, E.; Hiltner, A. *Appl. Phys. Lett.* **2004**, *84*, 3621–3623.

(31) Kimura, M.; Okahara, K.; Miyamoto, T. *J. Appl. Phys.* **1979**, *50*, 1222–1225.

(32) Álvarez, A. L.; Tito, J.; Vaello, M. B.; Velásquez, P.; Mallavia, R.; Sánchez-López, M. M.; Fernández de Ávila, S. *Thin Solid Films* **2003**, *433*, 277–280.

(33) Colodrero, S.; Mihi, A.; Anta, J. A.; Ocaña, M.; Mìguez, H. *J. Phys. Chem. C* **2009**, *113*, 1150–1154.

(34) Sánchez-Sobrado, O.; Yacomotti, A. M.; Calvo, M. E.; Martínez, O. E.; Ocaña, M.; Núñez, N.; Levenson, J. A.; Míguez, H. *Appl. Phys. Lett.* **2011**, *99*, 051111.

(35) Scotognella, F.; Monguzzi, A.; Cucini, M.; Meinardi, F.; Comoretto, D.; Tubino, R. *Int. J. Photoenergy* **2008**, *2008*, 389034.

(36) Puzzo, D. P.; Scotognella, F.; Zavelani-Rossi, M.; Sebastian, M.; Lough, J.; Manners, I.; Lanzani, G.; Tubino, R.; Ozin, G. A. *Nano Lett.* **2009**, *9*, 4273–4278.

(37) Scotognella, F.; Puzzo, D. P.; Monguzzi, A.; Wiersma, D. S.; Maschke, D.; Tubino, R.; Ozin, G. A. *Small* **2009**, *5*, 2048–2052.

(38) Bechger, L.; Lodahl, P.; Vos, W. L. *J. Phys. Chem. B* **2005**, *109*, 9980–9988.

(39) Morandi, V.; Marabelli, F.; Amendola, V.; Meneghetti, M.; Comoretto, D. *J. Phys. Chem. C* **2008**, *112*, 6293–6298.

(40) Morandi, V.; Marabelli, F.; Amendola, V.; Meneghetti, M.; Comoretto, D. *Adv. Funct. Mater.* **2007**, *17*, 2779–2786.

(41) Di Stasio, F.; Berti, L.; Burger, M.; Marabelli, F.; Gardin, S.; Dainese, T.; Signorini, R.; Bozio, R.; Comoretto, D. *Phys. Chem. Chem. Phys.* **2009**, *11*, 11515–11519.

(42) Zhang, Y.-Q.; Wang, J.-X.; Ji, Z.-Y.; Hu, W.-P.; Jiang, L.; Song, Y.-L.; Zhu, D.-B. *J. Mater. Chem.* **2007**, *17*, 90–94.

(43) Zhang, Q.; Bazuin, C. G.; Barrett, C. J. *Chem. Mater.* **2007**, *20*, 29–31.

(44) Vahala, K. J. *Nature* **2003**, *424*, 839–846.

(45) Notice that here we restrict our analysis to fully dielectric structures without comparing our results to planar microcavities where one of the mirrors is metallic.

(46) Ye, J. Y.; Ishikawa, M.; Yamane, Y.; Tsurumachi, N.; Nakatsuka, H. *Appl. Phys. Lett.* **1999**, *75*, 3605–3607.

(47) Hopmeier, M.; Guss, W.; Deussen, M.; Göbel, E. O.; Mahrt, R. F. *Phys. Rev. Lett.* **1999**, *82*, 4118–4121.

(48) Ozaki, R.; Matsuhisa, Y.; Ozaki, M.; Yoshino, K. *Appl. Phys. Lett.* **2004**, *84*, 1844–1846.

(49) Guo, L.; Krauss, T. D.; Poitras, C. B.; Lipson, M.; Teng, X.; Yang, H. *Appl. Phys. Lett.* **2006**, *89*, 061104.

(50) Persano, L.; Mele, E.; Cingolani, R.; Pisignano, D. *Appl. Phys. Lett.* **2005**, *87*, 031103.

(51) Kena Cohen, S.; Forrest, S. R. *Nat. Photonics* **2010**, *4*, 371–375.

(52) Burns, S. E.; Denton, G.; Tessler, N.; Stevens, M. A.; Cacialli, F.; Friend, R. H. *Opt. Mater.* **1998**, *9*, 18–24.

(53) Cacialli, F.; Hayes, G. R.; Grüner, J.; Phillips, R. T.; Friend, R. H. *Synth. Met.* **1997**, *84*, 533–534.

(54) Grüner, J.; Cacialli, F.; Friend, R. H. *J. Appl. Phys.* **1996**, *80*, 207–215.

(55) *Polymer Handbook*, 4th ed.; Brandrup, J. I., Immergut, E. H., Grulke, E. A., Abe, A.; Bloch, D. R., Ed.; John Wiley & Sons: New York, 2005.

(56) Warnecke, A. J.; LoPresti, P. J. *IBM J. Res. Dev.* **1973**, *17*, 256–262.

(57) *Handbook of Optical Constants of Solids*; Palik, E. D., Ed.; Elsevier: San Diego, CA, 1998.

(58) Moore, R. S. U.S. Patent no. 3,718,383, 1973.

(59) Ramsdale, C. M.; Greenham, N. C. *Adv. Mater.* **2002**, *14*, 212–215.

(60) Donley, C. L.; Zaumseil, J.; Andreasen, J. W.; Nielsen, M. M.; Sirringhaus, H.; Friend, R. H.; Kim, J.-S. *J. Am. Chem. Soc.* **2005**, *127*, 12890–12899.

(61) Stanley, R. P.; Houdr; eacute; R.; Oesterle, U.; Ilegems, M.; Weisbuch, C. *Phys. Rev. A* **1993**, *48*, 2246–2250.

(62) Keivanidis, P. E.; Kamm, V.; Dyer-Smith, C.; Zhang, W.; Laquai, F.; McCulloch, I.; Bradley, D. D. C.; Nelson, J. *Adv. Mater.* **2010**, *22*, 5183–5187.